Viscous Dynamics of Lyme Disease and Syphilis Spirochetes Reveal Flagellar Torque and Drag

Michael Harman,[†] Dhruv K. Vig,[†] Justin D. Radolf,[‡] and Charles W. Wolgemuth[†§¶*]

[†]University of Arizona, Department of Molecular and Cellular Biology, Tucson, Arizona; [‡]University of Connecticut Health Center, Departments of Medicine, Pediatrics, Genetics and Developmental Biology, Molecular Microbial and Structural Biology, and Immunology, Farmington, Connecticut; [§]University of Arizona, Department of Physics, Tucson, Arizona; and [¶]University of Connecticut Health Center, Department of Cell Biology and Center for Cell Analysis and Modeling, Farmington, Connecticut

ABSTRACT The spirochetes that cause Lyme disease (*Borrelia burgdorferi*) and syphilis (*Treponema pallidum*) swim through viscous fluids, such as blood and interstitial fluid, by undulating their bodies as traveling, planar waves. These undulations are driven by rotation of the flagella within the periplasmic space, the narrow (~20–40 nm in width) compartment between the inner and outer membranes. We show here that the swimming speeds of *B. burgdorferi* and *T. pallidum* decrease with increases in viscosity of the external aqueous milieu, even though the flagella are entirely intracellular. We then use mathematical modeling to show that the measured changes in speed are consistent with the exertion of constant torque by the spirochetal flagellar motors. Comparison of simulations, experiments, and a simple model for power dissipation allows us to estimate the torque and resistive drag that act on the flagella of these major spirochetal pathogens.

INTRODUCTION

Spirochetes are a unique phylum of eubacteria with many characteristics distinguishing them from the common Gram-positive or Gram-negative classifications (1,2). One striking difference is the means by which they swim. Like many other swimming bacteria, the spirochetes generate thrust against a fluid by rotating long helical filaments, known as flagella. However, spirochete flagella are internal, residing within the periplasm, the space between the inner and outer membranes (3,4). Therefore, the flagella are never in direct contact with the external fluid. Rotation of the flagella, which is driven by motors that are anchored near the ends of the bacteria, produces rotations and/or undulations of the entire bacterial cell body that propel these organisms through fluids (Fig. 1) (3,4).

It is also likely that undulation of the entire body of the bacterium allows spirochetes to wiggle through tight spaces, enabling them to penetrate dense, polymer-filled environments, such as the extracellular matrix (ECM), which can hinder the movement of externally flagellated bacteria (5,6). This unique mode of locomotion, then, may be a major reason why some of these bacteria are such successful pathogens (4,7). Indeed, two of the most invasive pathogens in humans are *Borrelia burgdorferi* (*Bb*) and *Treponema pallidum* (*Tp*), the bacteria that cause Lyme disease and syphilis, respectively (7,8). Interestingly, these two spirochetes both have flat-wave morphologies (9,10), planar, sinusoidal shapes distinguishing them from many other spirochetes, such as the oral commensal *Treponema denticola* and the *Leptospiraceae*, which are helical (11).

It is widely accepted that the motility of *Bb* and *Tp* is essential for the pathogenesis of both Lyme disease and syphilis (3,4). The transmission of *Bb* from its arthropod vector (the deer tick *Ixodes scapularis*) into the mammalian host, typically the white-footed mouse *Peromyscus leukopus* (7), requires the bacterium to exit the tick midgut by penetrating through the epithelium and a dense basement membrane (12). They then swim through the viscous hemolymph to the salivary glands, which they penetrate to access the salivary stream that transports them into the dermis of the mammal. Once within the skin, the clinical symptoms of Lyme disease are a direct manifestation of the spirochetes' ability to infiltrate and reside within the connective and soft tissues in which it incites tissue-damaging inflammatory responses. Acquisition of venereal syphilis occurs when *Tp* is inoculated into mucosa or skin, often in the genital or anorectal areas (13). *Tp* then rapidly disseminates, as exemplified by experiments in animals where treponemes were found in the blood, lymph nodes, bone marrow, spleen, and testes within 48 h after inoculation (14,15).

In humans, *Tp* also readily breaches the blood-brain barrier and infects the central nervous system (13). For both *Bb* and *Tp*, dissemination through the host requires traversing a range of circulatory and interstitial viscous fluids while withstanding shear and drag forces due to fluid flow. In addition, these bacteria cross many seemingly impenetrable barriers, such as basement membranes and endothelial layers. Many studies have examined the motility of *B. burgdorferi* in viscous media that roughly approximates the blood or hemolymph (see, for example, Goldstein et al. (9)); however, these investigations have not systematically studied the effect of viscosity on swimming dynamics. Viscous effects, though, are likely important, as recent work found that the speed with which the *Bb* migrates through

Submitted June 24, 2013, and accepted for publication October 8, 2013.

*Correspondence: wolg@email.arizona.edu

Michael Harman and Dhruv K. Vig contributed equally to this article.

Editor: Dennis Bray.

0006-3495/13/11/2273/8 $2.00

http://dx.doi.org/10.1016/j.bpj.2013.10.004

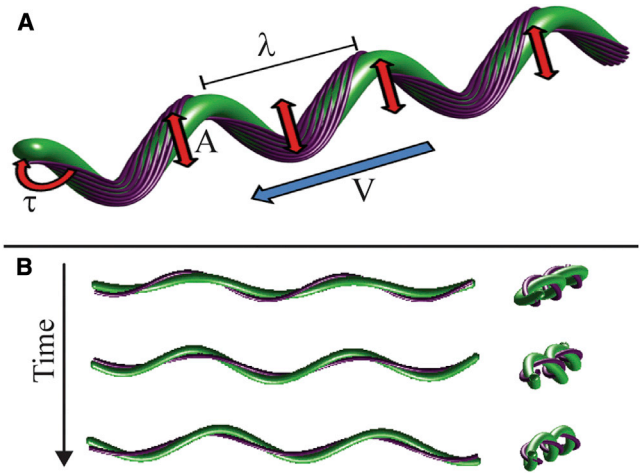

FIGURE 1 Schematic representation of swimming by a flat-wave spirochete. (*A*) The outer membrane has been removed to show how the helical flagella (*purple*), which are anchored into flagellar motors subterminally from the cell poles, wrap around the cell body. The cell body has a planar, sinusoidal appearance with wavelength, λ, and amplitude, A. A torque τ is applied to each flagellum, causing the flagella to rotate and the cell body to undulate. The traveling wave undulations of the cell body exert forces on the surrounding fluid that cause the bacterium to swim with velocity v. (*B*) Side and end-on views of frames from a simulation of *Bb* swimming in a viscous fluid. The waveform can be seen traveling toward the back of the cell as the cell rotates. To see this figure in color, go online.

the complex gel-like matrices that mimic the ECM is largely determined by the viscosity, not the elasticity, of the environment (16). Less is known about the motility of *T. pallidum*, as it is still not possible to culture this bacterium (17). However, the qualitative similarity between the shapes of *Bb* and *Tp* suggests that *B. burgdorferi* is a good model organism for understanding *Tp* motility in vivo.

Here we focus explicitly on the motility of *B. burgdorferi* and *T. pallidum* in viscous fluids to address two main questions:

First, how does the external viscosity of the environment affect the swimming of these spirochetes? Although it would seem likely that raising the external viscosity will impede the movement of these bacteria, the underlying physics is not clear, because the flagella are contained within the periplasmic space and the external viscosity cannot directly inhibit their rotation. If increasing the external viscosity slows the bacteria, can we understand the underlying physics and can we use this effect to estimate relevant biophysical parameters, such as the torque produced by the flagellar motor?

Second, in regard to motility, how similar are *B. burgdorferi* and *T. pallidum*? Both species have flat-wave morphologies, and the shape of *Bb* has been well characterized, having a wavelength of 3.1 μm and amplitude of 1.0 μm (9,18,19) (Fig. 1). In addition, both species contain multiple internal flagella (7–11 and 2–4 in *Bb* and *Tp*, respectively) that extend from motors attached at the ends of the cell and are long enough to overlap in the center (18–21)(Fig. 1). However, for *Bb* to be a model organism that is informative about *Tp* and syphilis pathogenesis, there needs to be convincing evidence that the motility-related biophysics of these two organisms operates under the same principles and responds similarly to the complex environments encountered in the host. Therefore, we address the question of whether or not the same biophysical model can explain the response of *Bb* and *Tp* to changes in external viscosity.

MATERIALS AND METHODS

Bacterial strains and media

Borrelia burgdorferi

All experiments with *B. burgdorferi* were done using the virulent, GFP-expressing strain Bb914 (parental strain 297) unless otherwise stated (12). Spirochetes were temperature-shifted to 37°C in BSK-II medium supplemented with 6% normal rabbit serum (Pel-Freeze Biologicals, Rogers, AK) and harvested in mid-log phase for imaging.

Treponema pallidum

Male New Zealand White rabbits (~3.5 kg), maintained on antibiotic-free food and water and housed at 16°C, were inoculated by injection of each testis with 1×10^8 *T. pallidum*. Ten days later, the animals were euthanized and the testes were aseptically removed. Several lengthwise cuts were made in each testis, after which the treponemes were extracted on a rotary shaker in CMRL 1066 (Invitrogen, Carlsbad, CA). Gross testicular contaminants were removed from the extract by centrifugation at 400 $\times$ *g* for 15 min. The animal protocols for this work were approved by the University of Connecticut Health Center Animal Care Committee and the Animal Care Committee of the Centers for Disease Control and Prevention under the auspices of Animal Welfare Assurance Nos. A3471-01 and A4365-01, respectively.

Ficoll solution preparation

A 45% stock solution of Ficoll PM-400 (Sigma-Aldrich, St. Louis, MO) was prepared in sterile phosphate-buffered saline by slowly dissolving 67.5 g of Ficoll powder into phosphate-buffered saline until reaching a final volume of 150 mL. This solution was autoclaved at 121°C for 25 min to ensure sterility. The appropriate volumes of this stock solution were diluted with sterile phosphate-buffered saline to produce 10-mL homogeneous solutions of the desired concentrations (1–30%). Solutions were stored at 4°C until the time of imaging.

Slide preparation

Small chambers were constructed with grease on clean slides to seal the samples and prevent environmental fluctuations. Spirochete cultures were diluted to ~2×10^7 cells/mL in media (BSK-II (*Bb*) or CMRL (*Tp*)), then mixed 1:1 with Ficoll solution to reach the desired final Ficoll concentration. A 70-μL quantity of this solution was plated in the chambers and a coverslip was carefully attached to prevent bubbles.

Microscopy setup

Images of spirochetes in media with or without Ficoll were captured at 40 frames/s on a BX41 microscope (Olympus, Melville, NY) equipped with a Retiga Exi Fast charge-coupled device camera (Qimaging, Burnaby, British Columbia, Canada) with the software STREAMPIX 3 (NorPix, Quebec,

Canada). Epifluorescent wide-field microscopy was used to capture images of *Bb* while dark-field illumination was used for *Tp*. Ten-second duration image sequences were captured with a 40× oil immersion objective to observe spirochete swimming and morphology. The image-plane was acquired nearly equidistant from the coverslip and glass slide to remove fluid effects near the chamber boundaries. Three separate experiments were performed for each spirochete/viscosity condition, with at least 100 bacterial trajectories captured during each trial. All imaging of *Tp* was done within 3 h of extraction.

Ficoll viscosity measurements

The stock Ficoll solutions were diluted 1:1 with BSK-II or CMRL medium to reach the appropriate working concentrations used during imaging. A quantity of 10 mL of solution was carefully added to a No. 2 size Gilmont Falling Ball Viscometer (Thermo Fisher Scientific, Waltham, MA) per the manufacturer's instructions. A glass bead was used for lower viscosity solutions (2–20 cP) and a stainless-steel bead was used for higher viscosities (10–100 cP). The time required for the bead to drop a set distance was recorded. Three separate trials were performed for each sample, and the average time, t, was used to calculate viscosity μ using the formula

$$\mu = K(\rho_c - \rho)t,$$

where K is a constant, ρ_c is the density of the bead, and ρ is the density of the solution. The drop time for the bead in water, which was assumed to have a viscosity of 1 cP, was used to determine the value of K. The same method was used to measure the viscosity of CMRL and BSK-II media without Ficoll. We found that both of these media have viscosities comparable to that of water.

Image analysis

Noise was removed from the image sequences using the software IMAGEJ (National Institutes of Health, Bethesda, MD) to enhance the contrast before analysis, and saved as uncompressed .avi files. An in-house tracking algorithm coded in the software MATLAB (The MathWorks, Natick, MA) was then utilized to extract the center of mass position, cell orientation, and the amplitude and wavelength of the flat-wave shape from the timelapse images, as previously described in Harman et al. (16). Velocity for spirochetes that remained in the field of view for at least 20 frames was then determined using the difference between the center-of-mass positions between subsequent frames. The average translocation velocity over the course of a time series was computed using the power spectrum of the Fourier transform of the velocity, extracting the dominant four modes. These modes were used to reconstruct a smoothed velocity from which the translocation velocity was defined as the maximum amplitude of this smoothed velocity. This maximum amplitude corresponds well with the speed of the cell during constant swimming (i.e., ignoring stops and reversals of direction), which was verified by a number of direct measurements of the speed during continuous swimming. The respective measurements were averaged across three separate experiments and the standard error of the mean was calculated.

Modeling the swimming dynamics of *B. burgdorferi* and *T. pallidum*

We used a previously developed model for the swimming dynamics of *B. burgdorferi* (22) to examine the effect of fluid viscosity on the undulation frequency of the Lyme disease and syphilis spirochetes. This model treats the cell body and periplasmic flagella of *Bb* and *Tp* as linear elastic filaments because they are significantly longer than they are wide (22,23). The dynamics of the cell are then calculated by balancing the elastic and resistive forces and moments that act among the cell, flagella, and external fluid. Movement of the cell body within a fluid is resisted by fluid drag, which is computed using resistive force theory (24). As in Vig and Wolgemuth (22), we treat the undulations of the cell body in the small amplitude regime and consider only motions perpendicular to the tangent vector of the cell body. Therefore, resistive forces between the fluid and the cell body are proportional to the velocity of the cell body, through the single drag coefficient $\zeta_\perp \sim 4\pi\eta$ (25), where η is the viscosity of the fluid. In addition, rotation of the cell body about its tangent vector is resisted by a torque proportional to the rotational speed, $\partial\phi/\partial t$; the rotational drag coefficient is $\zeta_r \sim 2a^2\eta$ (25).

Finally, rotation of the periplasmic flagella with respect to the cell body at angular speed ω_u experience resistive forces and moments that are proportional to ω_u (26). These forces and torques have the drag coefficients ζ_α and ζ_β, respectively (22). Collectively, this leads to the following force and moment equations (see Vig and Wolgemuth (22) for a complete derivation):

$$\begin{aligned}
\frac{\partial \mathbf{F}_c}{\partial x} + \mathbf{K} &= \zeta_\perp\left(\frac{\partial y}{dt}\hat{\mathbf{y}} + \frac{\partial z}{dt}\hat{\mathbf{z}}\right) - \zeta_\alpha a\left(\frac{\partial \alpha}{dt} - \frac{\partial \phi}{dt}\right)\hat{\mathbf{p}}_2,\\
\frac{\partial \mathbf{M}_c}{\partial x} + \hat{\mathbf{e}}_3 \times \mathbf{F}_c &= \left[\zeta_r\frac{\partial \phi}{dt} + \zeta_\alpha a^2\left(\frac{\partial \phi}{dt} - \frac{\partial \alpha}{dt}\right)\right]\hat{\mathbf{e}}_3,\\
\frac{\partial \mathbf{F}_f}{\partial x} - \mathbf{K} &= \zeta_\alpha a\left(\frac{\partial \alpha}{dt} - \frac{\partial \phi}{dt}\right)\hat{\mathbf{p}}_2,\\
\frac{\partial \mathbf{M}_f}{\partial x} + \hat{\mathbf{e}}_3 \times \mathbf{F}_f &= \zeta_\beta \omega_u \hat{\mathbf{e}}_3,
\end{aligned} \tag{1}$$

where $\mathbf{F}_c$ and $\mathbf{M}_c$ and $\mathbf{F}_f$ and $\mathbf{M}_f$ are the forces and torques on the cell body and flagella, respectively; $\hat{\mathbf{p}}_1$ is the direction from the centerline of the cell body to the flagella; and $\hat{\mathbf{p}}_2 = \hat{\mathbf{x}} \times \hat{\mathbf{p}}_1$. The normal forces between the flagella and the cell body, $\mathbf{K}$, point in the direction $-\hat{\mathbf{p}}_1$.

The dynamics of *Bb* and *Tp* were simulated by solving the expressions in Eq. 1 using a fourth-order, finite-difference spatial discretization and a semi-implicit time-stepping routine (22). Simulations were performed in the software MATLAB using a spatial discretization of 100-300 nodes and a time-step of $10^{-7} - 10^{-6}$s, with each run simulated for a total time of 10 s. For simulations that corresponded to *Bb*, the bending moduli of the cell body and periplasmic flagella were defined using experimentally measured values for *Bb* (22,23).

The diameter of the cell body of *Tp* is roughly half that of *Bb*, and *Tp* has only two flagella per end (10). For simulations corresponding to *Tp*, we therefore used cell body and flagellar bending moduli that were fourfold smaller than those of *Bb* (the bending modulus scales roughly like the cube of the cell diameter). Our experiments determined that the wavelength and amplitude of *Tp* were 1.56 and 0.44 μm, respectively (see Results and Discussion). To approximate this shape in our simulations, we set the preferred curvature and torsion of the flagella to be 2 and 3 μm^{-1}, respectively. With these values, our simulations produced a flat-wave shape with a wavelength of ~2 μm and amplitude of ~0.4 μm. We, therefore, expect that the shape of purified *Tp* flagella should have a curvature of ~2 μm^{-1} and torsion of ~3 μm^{-1}.

The value of ζ_β is not known. Therefore, we used a range of values between 10^{-6} and 10^{-2} pN s for our simulations. For each value of ζ_β, we determined the value of the torque τ that resulted in an undulation frequency of 10 Hz when the fluid viscosity was equal to that of water. We then used these values of τ to determine how the undulation frequencies depended on external viscosity.

RESULTS AND DISCUSSION

To determine how the swimming speeds of *Bb* and *Tp* were affected by the viscosity of the environment, we used Ficoll, a hydrophilic polysaccharide that readily dissolves in

solution, to increase medium viscosity. We chose Ficoll because it has been shown to increase the viscosity of a solution without producing non-Newtonian effects (i.e., the fluid remains Newtonian with the stress in the fluid being proportional to the gradient of the velocity) (27). We varied the Ficoll concentrations from 0 to 30% (wt/vol) and found that, in general and as expected, the speed of *Bb* and *Tp* decreased with increases in Ficoll concentration (Figs. 2 and 3 *E*). These Ficoll concentrations represent a range of viscosities from 1 to 50 times the viscosity of water (Fig. 3 *E*, *inset*), which is characteristic of the viscosities that spirochetes encounter in biologic fluids, such as blood (28). For *Bb*, we found that the speed in BSK-II medium without Ficoll was 6.8 ± 0.4 μm/s, which is consistent with previous measurements (9). The 1% Ficoll solutions showed a marked decrease in speed (3.1 ± 0.2 μm/s), which may have been due to the fact that this data set included fewer measurements and there was a noticeable day-to-day variation in the average swim speed of the spirochetes. At higher concentrations of Ficoll, the speed of *Bb* decreased from 5.9 ± 0.4 μm/s in 6% solutions to 3.5 ± 0.3 μm/s in 20% solutions. Compared to *Bb*, the swimming speed of *Tp* was more strongly affected by Ficoll concentration, which is likely due to the fact that *Tp* is thinner and has fewer flagella (10). In CMRL medium without Ficoll, the average swimming speed of *Tp* was 1.9 ± 0.2 μm/s; this value dropped monotonically to 1.3 ± 0.1 μm/s in 9% solutions. We were unable to accurately measure speeds below ~0.8 μm/s and, therefore, did not examine the motility of *Tp* in solutions above 9% Ficoll.

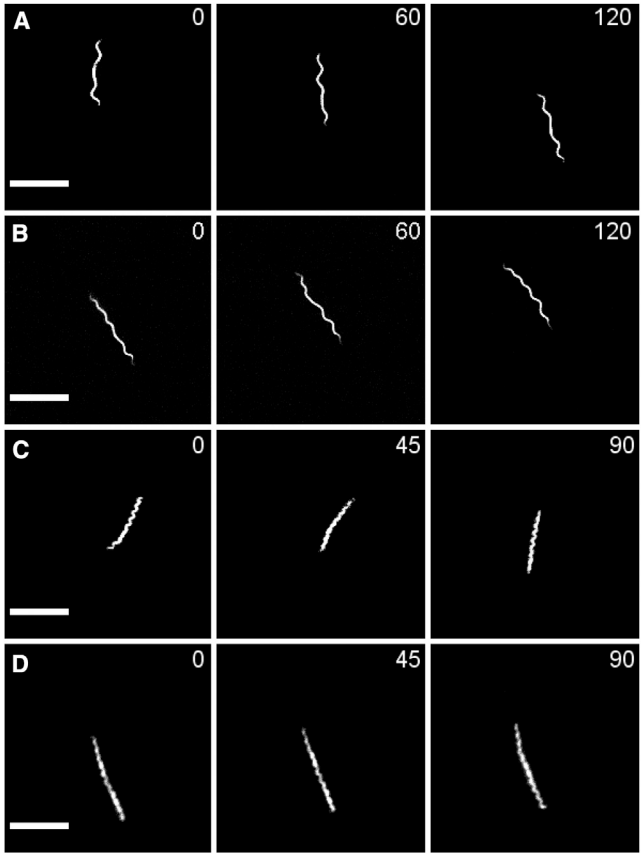

FIGURE 2 Time courses of *Bb* and *Tp* swimming in liquid growth media and in Ficoll solutions. In BSK-II medium (*A*), *Bb* makes noticeably larger net displacement in 6.0 s than in 20% Ficoll solution (*B*). *Tp* shows similar behavior, swimming farther in CMRL medium (*C*) than in 9% Ficoll solution (*D*), where there is minimal net displacement. Frame numbers are given in the top-right corner, with a time step of ~0.05 s/frame. Scale bar = 10 μm.

At low Reynolds number, the speed of a thin swimmer that produces traveling wave undulations depends only on the wavelength (λ), amplitude (A), and undulation frequency (ω) (29,30). We, therefore, sought to determine which of these parameters was affected by changes in the external viscosity. We measured the wavelength and amplitude of *Bb* and *Tp* as a function of Ficoll concentration and found that the average wavelength and amplitude of *Bb* (3.29 ± 0.07 μm and 0.77 ± 0.03 μm, respectively) and *Tp* (1.56 ± 0.04 μm and 0.28 ± 0.01 μm, respectively) did not change with viscosity (Fig. 3, *A–D*). Our measurements of the wavelength of *Bb* are consistent with previous measurements from the literature (9,16,18,23). The value reported herein for the amplitude is lower than that previously reported, which is likely due to the fact that we did not selectively analyze frames where the flat-wave is in the imaging plane. Our value for the amplitude, therefore, represents an average over all possible orientations. Assuming equal probabilities for all orientations, we estimate that the actual amplitude is $\pi/2$ times larger, or 1.21 ± 0.04 μm, which agrees well with previous reports (9,18,23). By similar reasoning, we expect that the actual amplitude of *Tp* is 0.44 ± 0.01 μm. To our knowledge, this is the first time that the speed, wavelength, and amplitude of *Tp* have been reported. It is interesting to note that wavelength/amplitude for *Bb* and *Tp* is nearly identical (~3). These values are very close to π, the optimal ratio that maximizes swimming speed at fixed frequency, which can be shown by optimizing the speed with respect to λ/A using resistive force theory (16,30).

Because the wavelength and amplitude are not affected by viscosity, the decrease in swimming speed must be due to a decrease in the undulation rate of the spirochetes, which is predicted to be the same as the rotational speed of the flagella (22). Therefore, increasing the external viscosity slows the rotation of the flagella, which are never in contact with the external environment. A similar effect was recently observed for *Bb* swimming through gelatin matrices, and a power balance argument was used to suggest that the affect on the speed was only influenced by the viscosity of the gelatin matrices, not the elasticity (16). This power balance argument attempts to side-step the complexity of the swimming mechanism of the spirochetes by considering only the power that is put in by the flagellar motors to drive motility and the power dissipated by the movement of the spirochete through the fluid. Specifically, the power input by the motors

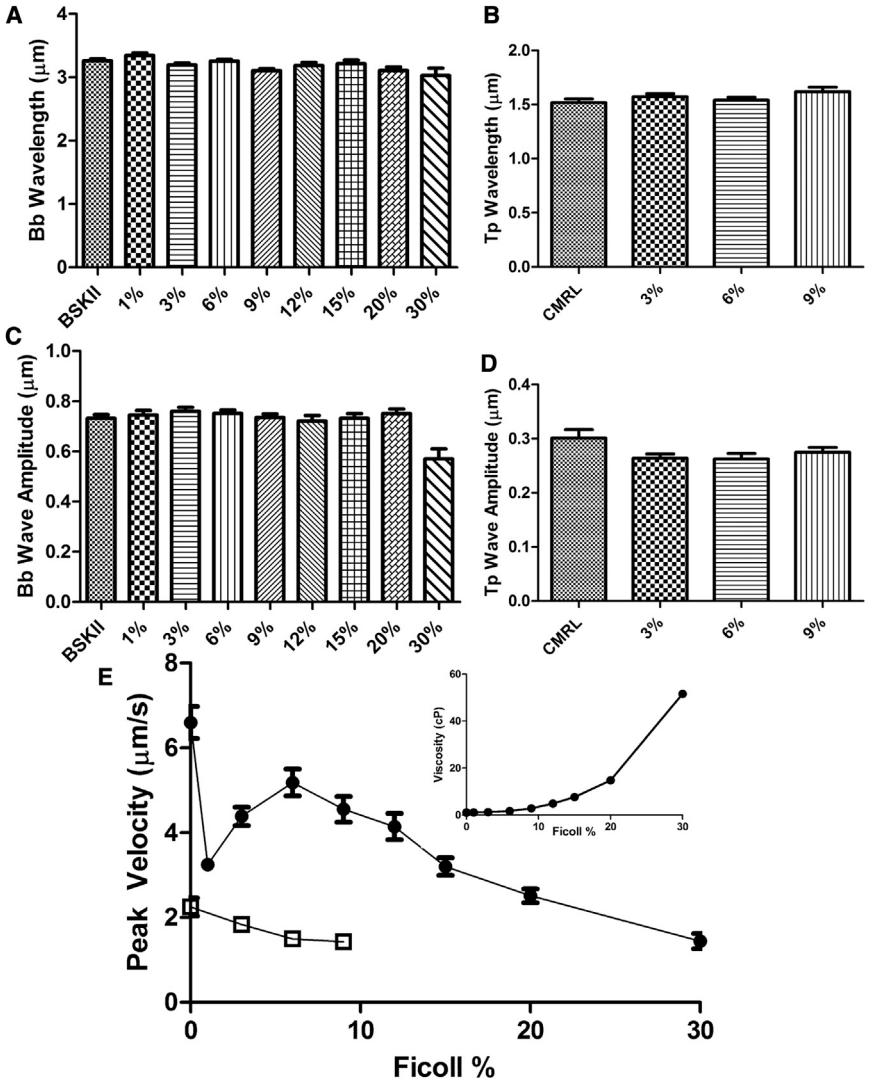

FIGURE 3 Quantitative analysis of spirochetes swimming at varying viscosities. The wavelengths of *Bb* (*A*) and *Tp* (*B*) do not change significantly with changes in Ficoll concentration. Likewise, there are not significant changes in the amplitudes of *Bb* (*C*) or *Tp* (*D*) with changes in Ficoll concentration. (*E*) The peak swimming velocity for *Bb* (*solid circles*) and *Tp* (*open squares*) decreases with viscosity. (*Inset*) Dependence of fluid viscosity on Ficoll concentration.

is equal to the product of the number of motors, N, the torque per motor, τ, and the rotational speed, ω. Power is predominantly dissipated in two ways:

1. By rotation of the flagella in the periplasm, where the power dissipated is proportional to the number of flagella, the length of the flagella (L), the square of the rotational speed, and a drag coefficient (ζ_β) (26); and
2. By undulation of the cell body through the surrounding fluid, in which we equate the power in with the power dissipated,

$$\underbrace{N\tau\omega}_{\text{Power in}} = \underbrace{N\zeta_\beta L\omega^2 + \frac{1}{8}\zeta_\perp LA^2\omega^2}_{\text{Power dissipated}}, \qquad (2)$$

where $\zeta_\perp \approx 4\pi\eta$ is the perpendicular drag coefficient with η the viscosity (25).

We have assumed that we can neglect dissipation due to the swimming speed compared to the undulation speed, because the undulation speed is roughly 5–10 times the swimming speed (9). Our solutions are purely viscous, which suggests that the power balance argument should be directly applicable to our experiments and, furthermore, allows us to accurately estimate the drag coefficients that describe the resistive forces that act against the undulating bacterium. Because the wavelength and amplitude are constants, we can rewrite this equation in terms of the swimming speed which is proportional to the rotational rate, $v = c\omega$, where c is a constant that is = ~0.05 μm. Therefore, we expect that the relationship between the swimming speed and the viscosity should be

$$\frac{1}{v} = \frac{1}{c}\left(\frac{\zeta_\beta L}{\tau} + \left(\frac{\pi A^2 L}{2N\tau}\right)\eta\right), \qquad (3)$$

which predicts that the inverse of the velocity is linearly related to the viscosity. In addition, this relationship predicts that the slope of the inverse velocity with respect to viscosity is inversely related to the number of flagella and will,

therefore, be steeper for *Tp* than for *Bb*, assuming that the torques from the flagellar motors are the same in these bacteria. In addition, using this relationship, it should be possible to estimate the torque from the flagellar motor and the drag coefficient for rotating the flagella in the periplasmic space.

To test the predictions of Eq. 3, we replotted our data as the inverse swimming speed of *Bb* and *Tp* with respect to viscosity (Fig. 4). For both species there is an approximately linear relationship with slopes of 0.011 μm/pN (*Bb*) and 0.13 μm/pN (*Tp*) and *y* intercepts of 0.21 s/μm (*Bb*) and 0.36 s/μm (*Tp*); however, the plots for both species also show some concavity. Some of the deviation from linearity observed in the *Tp* data may be due to the fact that the average velocity in the highest viscosity solution approaches the limits of our measurement resolution. As predicted by power balance, the average slope of the *Tp* data is steeper than that of *Bb*. Therefore, there is at least qualitative agreement between the Eq. 3 and our data. We would like to be able to use these slopes to determine the flagellar motor torques, with the *y* intercepts then giving the periplasmic drag coefficients.

Using the known values for the amplitudes and estimates for the length and number of flagella of 10 μm and 10 for *Bb*, and 10 μm and 2 for *Tp*, respectively, we estimate the torques to be 2700 pN nm for *Bb* and 800 pN nm for *Tp*, which are within the range of values of the stall torques measured in *Caulobacter crescentus* and *Escherichia coli* (350 and 4500 pN nm, respectively) (31,32). Using these values for the torque, along with our values of the *y* intercepts, we estimate that the drag coefficients for rotating the flagella in the periplasm is ~3.0×10^{-3} pN s for *Bb* and slightly lower, 7.0×10^{-4} pN s, for *Tp*. However, it is not clear whether the power balance equation can be used to give quantitative information regarding these values.

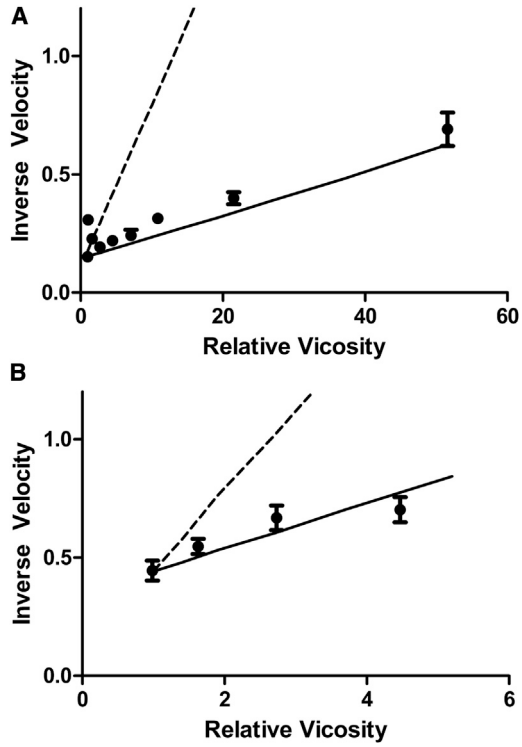

FIGURE 4 Inverse velocity (s/μm) versus viscosity for *Bb* (*A*) and *Tp* (*B*). (*Solid circles*) Experimental results and the lines show predictions from our model with $\zeta_\beta = 10^{-2}$ pN s (*solid line*) and10^{-3} pN s (*dashed line*) for *Bb*, and $\zeta_\beta = 10^{-3}$ pN s (*solid line*) and 10^{-4} pN s (*dashed line*) for *Tp*. Viscosity is relative to that of water, which is assumed to have a viscosity of 0.001 Pa s.

To determine the accuracy of the torque and drag coefficients predicted from the power balance equation, we used the biophysical model for *Bb* swimming that was developed by Vig and Wolgemuth (22) to explore how changes in viscosity affected the undulation frequency. We simulated flat-wave spirochetes swimming through fluids with a range of viscosities, as described in the Materials and Methods (Fig. 1 *B*). We mimicked the difference between *Tp* and *Bb* by adjusting the preferred shape of the flagella, the flagellar stiffness, and the total torque applied to the flagella. For a given torque and viscosity, the simulation predicts the undulation frequency of the spirochete. We then estimated the swimming speed from the undulation frequency using that $v = c\omega$ and plotted the inverse velocity as a function of viscosity (Fig. 4 *B*). As in our experiments, we always found a roughly linear, monotonic increase in the inverse velocity with increases in the viscosity. The biophysical model shows a complex relationship between the velocity of the cell body and the forces and torques that are exerted back on the flagella.

In effect, viscous resistance from the external fluid exerts forces on the cell body that are transmitted to the flagella via the resistive forces from the periplasmic fluid and normal forces from the outer membrane and cell wall. The resulting forces and torques on the flagella resist the torque from the flagellar motors, causing the rotation of the motors to slow down as the viscosity is increased. Our simulations that represented *Tp* also showed a steeper slope than the simulations of *Bb*, and for some simulations, the relationship between the inverse velocity and viscosity showed concavity for larger values of the flagellar drag coefficient ζ_β. Therefore, our simulations are in qualitative agreement with our experiments and with the predictions from Eq. 3. However, we know the torque and drag coefficients that were used in the simulations. We, therefore, fit our simulated data to the results from Eq. 3 and extracted the torque and drag coefficients using the same procedure that we used for our experimental data. For all values of the torque and drag coefficients that we used in our simulations, we found that the values predicted from the power balance equation were always within a factor of 5 of the input parameters. Furthermore, we found that for lower values of ζ_β, the estimate of the torque was more accurate. In addition, the values for the torque computed using the power balance equation

were always overestimates for the value that we imposed in our simulations, which suggests that the value for the torque that we calculated using our experimental data represents an upper limit on the actual torque.

We then fit our simulated data to our experimental data (Fig. 4). Our simulations match the data well for *Bb* with a torque value of 1300 pN nm and $\zeta_\beta = 10^{-2}$ pN s. For *Tp*, we find good agreement with our experiments with a torque of 500 pN nm and $\zeta_\beta = 10^{-3}$ pN s. Because our simulations treat the flagellar ribbon as a single flagellum, we expect that these values represent the total torque and drag coefficient. Obtaining the values for a single flagellum requires dividing these numbers by the number of flagella. Therefore, our simulations suggest that the torque and drag coefficient for *Bb* are ~200 pN nm and ~1.5×10^{-3} pN s, respectively, and for *Tp* ~ 250 pN nm and 5×10^{-4} pN s, respectively. In both cases, we find that the values are within the same order of magnitude as those predicted by the power equation.

In this study, we set out to examine two questions:

The first question that we asked was how the swimming speeds of *Bb* and *Tp* were affected by external viscosity, and whether this effect could be used to determine the torque from the flagellar motor. We showed that changes in external viscosity slowed down the spirochetes. Then, by considering the power balance during swimming, we predicted that the velocity should vary inversely with viscosity. Comparing our experimental data to the simple power balance equation (Eq. 3) and to a more complete biophysical model for the swimming of spirochetes, we were able to estimate the torque that is produced by the flagellar motors of the Lyme disease and syphilis spirochetes. In addition, we were able to estimate the drag coefficient for rotating the flagella in the periplasmic space, a value that will be potentially difficult to measure experimentally. Our value for this drag coefficient is in rough agreement with theoretical predictions for the drag coefficient in *Bb* that were based on Stokes flow around a rotating cylinder confined between two walls (26). In addition, the similarity between the observed decrease in speed with viscosity and the predictions from the biophysical model of Vig and Wolgemuth (22) provides further support for the relevance of this model of flat-wave spirochete swimming. Our results also suggest that the flagellar motor of these two spirochete species produces a constant torque that is independent of rotational speed, as is assumed in our biophysical model and has been shown for the flagellar motors of *E. coli* and *C. crescentus* (27,31).

The second question that we addressed was how the swimming behavior of *Bb* compares with that of *Tp* in viscous fluids. Our analysis showed that both these organisms respond to changes in viscosity in a similar manner and could be explained by the same biophysical model. The inability to culture *Tp* prevents constructing genetically modified strains, such as ones that express fluorescent markers, which would enable the study of the invasion and dissemination of *Tp* through environments that better resemble the diversity of the host milieu. These types of experiments, however, are possible and have been done with *Bb* (16). As both of these spirochetes migrate through the ECM and penetrate intracellular junctions in the mammalian host, it is attractive to consider *Bb* as a good model for *Tp*. While previous researchers have related *Bb* to *Tp* based primarily on morphological similarities, invasion and dissemination through the host requires similarities in motility. Although there is a notable difference in the range of viscosities over which these organisms can swim, our results suggest that this can be attributed to the greater number of flagella in *Bb* than in *Tp*. Therefore, the work presented here provides further evidence that *Bb* is a good model organism for understanding some aspects of the pathogenesis of syphilis, while also providing clearer insight into Lyme disease.

The authors thank Morgan Lavake and Carson Karanian for performing the *Tp* extractions.

This research was supported by National Institutes of Health grant Nos. R01GM072004 (to C.W.W.), R01AI029735 (to J.D.R.), 3R01AI29735-20S1 (to J.D.R.), and R01AI26756 (to J.D.R.).

REFERENCES

1. Paster, B. J., and F. E. Dewhirst. 2000. Phylogenetic foundation of spirochetes. *J. Mol. Microbiol. Biotechnol.* 2:341–344.
2. Bergstrom, S., and W. R. Zuckert. 2010. Structure, function and biogenesis of the *Borrelia* cell envelope. *In Borrelia*: Molecular Biology, Host Interaction and Pathogenesis. D. S. Samuels and J. D. Radolf, editors. Caister Academic Press, Norfolk, United Kingdom.
3. Charon, N. W., A. Cockburn, …, C. W. Wolgemuth. 2012. The unique paradigm of spirochete motility and chemotaxis. *Annu. Rev. Microbiol.* 66:349–370.
4. Charon, N. W., and S. F. Goldstein. 2002. Genetics of motility and chemotaxis of a fascinating group of bacteria: the spirochetes. *Annu. Rev. Genet.* 36:47–73.
5. Kimsey, R. B., and A. Spielman. 1990. Motility of Lyme disease spirochetes in fluids as viscous as the extracellular matrix. *J. Infect. Dis.* 162:1205–1208.
6. Berg, H. C., and L. Turner. 1979. Movement of microorganisms in viscous environments. *Nature.* 278:349–351.
7. Radolf, J. D., M. J. Caimano, …, L. T. Hu. 2012. Of ticks, mice and men: understanding the dual-host lifestyle of Lyme disease spirochetes. *Nat. Rev. Microbiol.* 10:87–99.
8. Singh, A. E., and B. Romanowski. 1999. Syphilis: review with emphasis on clinical, epidemiologic, and some biologic features. *Clin. Microbiol. Rev.* 12:187–209.
9. Goldstein, S. F., N. W. Charon, and J. A. Kreiling. 1994. *Borrelia burgdorferi* swims with a planar waveform similar to that of eukaryotic flagella. *Proc. Natl. Acad. Sci. USA.* 91:3433–3437.
10. Izard, J., C. Renken, …, J. D. Radolf. 2009. Cryo-electron tomography elucidates the molecular architecture of *Treponema pallidum*, the syphilis spirochete. *J. Bacteriol.* 191:7566–7580.
11. Wolgemuth, C. W., N. W. Charon, …, R. E. Goldstein. 2006. The flagellar cytoskeleton of the spirochetes. *J. Mol. Microbiol. Biotechnol.* 11:221–227.

12. Dunham-Ems, S. M., M. J. Caimano, …, J. D. Radolf. 2009. Live imaging reveals a biphasic mode of dissemination of *Borrelia burgdorferi* within ticks. *J. Clin. Invest.* 119:3652–3665.

13. Radolf, J. D., K. R. O. Hazlett, and S. A. Lukehart. 2006. Pathogenesis of syphilis. *In* Pathogenic *Treponema*: Molecular and Cellular Biology. J. D. Radolf and S. A. Lukehart, editors. Caister Academic Press, Norfolk, United Kingdom.

14. Stokes, J. H., H. Beerman, and N. R. Ingraham. 1944. Modern Clinical Syphilology. W.B. Saunders, Philadelphia, PA.

15. Brown, W. H., and L. Pearce. 1920. A note on the dissemination of *Spirochaeta pallida* from the primary focus of infection. *Arch. Derm. Syphilol.* 2:470–472.

16. Harman, M. W., S. M. Dunham-Ems, …, C. W. Wolgemuth. 2012. The heterogeneous motility of the Lyme disease spirochete in gelatin mimics dissemination through tissue. *Proc. Natl. Acad. Sci. USA.* 109:3059–3064.

17. Cox, D. L., and J. D. Radolf. 2006. Metabolism of the *Treponema*. *In* Pathogenic *Treponema*: Molecular and Cellular Biology. J. D. Radolf and S. A. Lukehart, editors. Caister Academic Press, Norfolk, United Kingdom.

18. Goldstein, S. F., K. F. Buttle, and N. W. Charon. 1996. Structural analysis of the *Leptospiraceae* and *Borrelia burgdorferi* by high-voltage electron microscopy. *J. Bacteriol.* 178:6539–6545.

19. Hovind-Hougen, K. 1984. Ultrastructure of spirochetes isolated from *Ixodes ricinus* and *Ixodes dammini*. *Yale J. Biol. Med.* 57:543–548.

20. Kudryashev, M., M. Cyrklaff, …, F. Frischknecht. 2009. Comparative cryo-electron tomography of pathogenic Lyme disease spirochetes. *Mol. Microbiol.* 71:1415–1434.

21. Liu, J., T. Lin, …, S. J. Norris. 2009. Intact flagellar motor of *Borrelia burgdorferi* revealed by cryo-electron tomography: evidence for stator ring curvature and rotor/C-ring assembly flexion. *J. Bacteriol.* 191:5026–5036.

22. Vig, D. K., and C. W. Wolgemuth. 2012. Swimming dynamics of the Lyme disease spirochete. *Phys. Rev. Lett.* 109:218104.

23. Dombrowski, C., W. Kan, …, C. W. Wolgemuth. 2009. The elastic basis for the shape of *Borrelia burgdorferi*. *Biophys. J.* 96:4409–4417.

24. Gray, J., and G. J. Hancock. 1955. The propulsion of sea-urchin spermatozoa. *J. Exp. Biol.* 32:802–814.

25. Keller, J., and S. Rubinow. 1976. Slender-body theory for slow viscous flow. *J. Fluid Mech.* 44:705–714.

26. Yang, J., G. Huber, and C. W. Wolgemuth. 2011. Forces and torques on rotating spirochete flagella. *Phys. Rev. Lett.* 107:268101.

27. Chen, X., and H. C. Berg. 2000. Torque-speed relationship of the flagellar rotary motor of *Escherichia coli*. *Biophys. J.* 78:1036–1041.

28. Windberger, U., A. Bartholovitsch, …, G. Heinze. 2003. Whole blood viscosity, plasma viscosity and erythrocyte aggregation in nine mammalian species: reference values and comparison of data. *Exp. Physiol.* 88:431–440.

29. Taylor, G. I. 1952. The action of waving cylindrical tails in propelling microorganisms. *Proc. R. Soc. Lond. A Math. Phys. Sci.* 211:225–239.

30. Chwang, A. T., H. Winet, and T. Y. Wu. 1974. A theoretical mechanism of spirochete locomotion. *J. Mechanochem. Cell Motil.* 3:69–76.

31. Li, G., and J. X. Tang. 2006. Low flagellar motor torque and high swimming efficiency of *Caulobacter crescentus* swarmer cells. *Biophys. J.* 91:2726–2734.

32. Berry, R. M., and H. C. Berg. 1997. Absence of a barrier to backwards rotation of the bacterial flagellar motor demonstrated with optical tweezers. *Proc. Natl. Acad. Sci. USA.* 94:14433–14437.